An ultra-compact metasurface and specklemeter based chromatic confocal sensor

Przemyslaw Falak, Justin Ho-Tin Chan, James Williamson, Andrew Henning, Timothy Lee, Shahrzad Zahertar, Christopher Holmes, Martynas Beresna, Haydn Martin, Gilberto Brambilla, and Xiangqian Jiang

Abstract—The development of ultra-compact lightweight optical instrumentation that can be used on-machine and to carry out in-process measurements is vital in realizing improved manufacturing processes, increasing the quality of parts being made while saving time and energy by reducing scrappage rates. Only incremental progress is being made in developing suitable instrumentation based on conventional components such as traditional refractive elements as fundamental limits in terms of size and weight are already reached. Here we demonstrate a chromatic confocal sensor that utilizes the natural chromatic aberration found with a basic hyperbolic metalens to realize an ultra-compact and simple probe. Further, we demonstrate how this can be combined with a compact specklemeter as the detection element, thus realizing the whole sensing system in a compact manner. Even with the proof-of-principle instrument in its preliminary and unoptimised state we achieve the successful recovery of the location of a scatterer as it is scanned over a 227 μm range, with a standard deviation of error in the position of 1.37 μm. Sensors of this form can be deployed in areas where traditional instrumentation would typically impede the manufacturing processes, increasing the number of processes that can have metrology applied directly and providing real-time feedback to improve manufacturing outcomes.

Index Terms—Chromatic confocal sensors, laser-writing, metalens, scattering flat fiber, speckle patterns

I. INTRODUCTION

There has recently been significant interest to implement metrology in a manner that can deliver on-machine [1]–[3] and, ideally, real-time in-process [4], [5] measurements to provide feedback during manufacturing. By proliferating small and lightweight sensors to provide the required feedback, the realisation of smart and autonomous processes would be possible [6]. This would allow bespoke one-off items to be made without the significant trial-and-error steps needed to refine the process and correct for errors, and would allow more consistent items to be produced when carrying out larger runs, in both cases reducing scrappage rates and saving time and energy [7]. Unfortunately, most optical instrumentation currently available is too bulky and heavy for this purpose, and new approaches need to be sought to realise it in an ultra-compact and lightweight form that will allow it to be deployed in the space available without interfering with other processes [8], [9].

P. F., T. L., C. H., S. Z., M. B., and G.B. are with the Optoelectronics Research Centre, University of Southampton, Southampton, SO17 1BJ, United Kingdom (e-mail: p.falak@soton.ac.uk).

J. C., J. W., A. H., H. M., and X. J. are with the Centre for Precision Technologies, University of Huddersfield, Huddersfield, HD1 3DH, United Kingdom, (e-mail: a.henning@hud.ac.uk).

Chromatic confocal sensing (CCS) [10] is ideal for many measurement tasks [11] as it measures the location of a surface without the need to mechanically scan any elements, and the simple signal that they generate allows for high-speed signal processing to be carried out. As such, it has recently been deployed in numerous applications such as for on-machine measurements on diamond turning machines [12], [13], for layer thickness measurements [14], to carry out measurements when using micro-EDM drilling and milling machines [15], and for in-situ measurements of surface roughness [16] and if greater compactness is achieved still more applications will open up as, while it has been deployed in these applications, the chromatic confocal probes are still currently unwieldy.

In this technique the sensor effectively acts as a set of confocal probes [17]–[21] being used in parallel, each utilising a different wavelength of light and focussing it to a different point after the lens. This leads to the position of a measurand filtering the incident broadband light such that only a narrow band is returned, and whose wavelengths are dependent on the surface location. By determining the wavelength most strongly returned using a combination of a spectrometer and the application of a simple peak fitting algorithm, the location of the measurand is immediately obtained. By applying a beam-scanning approach it is also possible to produce both surface topography and form information.

The wavelength filtering process is achieved by using a probe that focuses different wavelengths to different points along the optical axis i.e. it imparts substantial logitudinal chromatic aberration (LCA) by design. Typically, this may be done in a couple of different manners, such as using groups of lenses or hyperchromatic diffractive optical elements (DOEs). When a group of lenses are used, they take up significant space, restricting how much the instrument can be miniaturized, while hyperchromatic DOEs are large, complex, and difficult to manufacture. However, particularly relevant to this work is the observation that basic hyperbolic metalenses can possess significant chromatic aberration which is an inherent aspect of their operation. In many applications this is considered a disadvantage, but for CCS we have shown it can be used to realize the required spectral filtering when combined with a pinhole, and the planar and compact nature of the metasurface presents substantial advantage with regard to potential miniaturization of the front-end probe. While in [22] we demonstrated this functionality using a metasurface designed to focus a collimated beam of light, here we present an improved design that focuses the light directly from the end of an optical fibre. This removes the need for an additional

collimator and greatly reduces the size and the weight of the probe.

While this metasurface implementation of the probe allows it to be realised in an ultra-compact form, the vision for an ultra-compact and low cost CCS sensor is not achievable without also addressing the size of the detection element, as conventional spectrometers represent a large part of the overall system cost and bulk. Here we propose replacing the spectrometer with a specklemeter, a device that uses the highly wavelength dependant speckle pattern produced when light passes through a disordered medium to determine its wavelength [23], [24]. This is a compact and low cost element that can be realised in a highly compact form directly on the end of an optical fibre. The specklemeter in this work is formed by laser writing a pseudo-randomized set of scattering voids into a section of fused quartz flat fiber [25]–[27] spliced onto the end of the single mode optical fibre that the light to be analysed is passing through. While such devices work best with monochromatic light, as broadband light will wash out the speckles generated, here we demonstrate that the band of light filtered from the broadband light source by the metasurface based probe is narrow enough to still allow its use in this application, successfully allowing the retrieval of the location of the scatterer from the speckle pattern produced. While the specklemeter may be used to determine the spectral content of the light returned into the system, in this work we circumvent this step by directly relating the location of the scatterer to the speckle pattern produced. This approach allows the entire sensor to be realized in a low-cost and miniaturised form, allowing for its deployment in a broad range of applications where the size and cost of currently available instrumentation is prohibitive.

II. THE CHROMATIC CONFOCAL METALENS PROBE

A. Design, function and construction of the probe

A CCS probe takes broadband light as an input and after scattering the light from the object of interest, only a narrow band of light is collected whose wavelengths depend on the scatterer's location. Thus, to determine the location of the scatterer, all that is needed is to find the wavelength of light most strongly returned. An illustration of such a probe is shown in fig. 1. Here the metasurface-based probe takes light from a point source which, in this case, is the aperture of a single-mode optical fiber. The LCA afforded by the metasurface results in different wavelengths of light being focused into unique positions along the optical axis. Fig.1. parts (b) and (c) illustrate how different portions of the incident light is filtered when scattering from a mirror located at different distances away from the probe. While all of the illuminating light is reflected from the measurand, only those wavelengths that were in optimal focus at the mirror surface will be focused back onto the fiber aperture and thus effectively couple back in. The wavelengths of light that are out of focus on the mirror surface are also out of focus on the plane containing fiber aperture after scattering.

While we have recently demonstrated that a basic single-surface hyperbolic metalens can also be used, however, in that
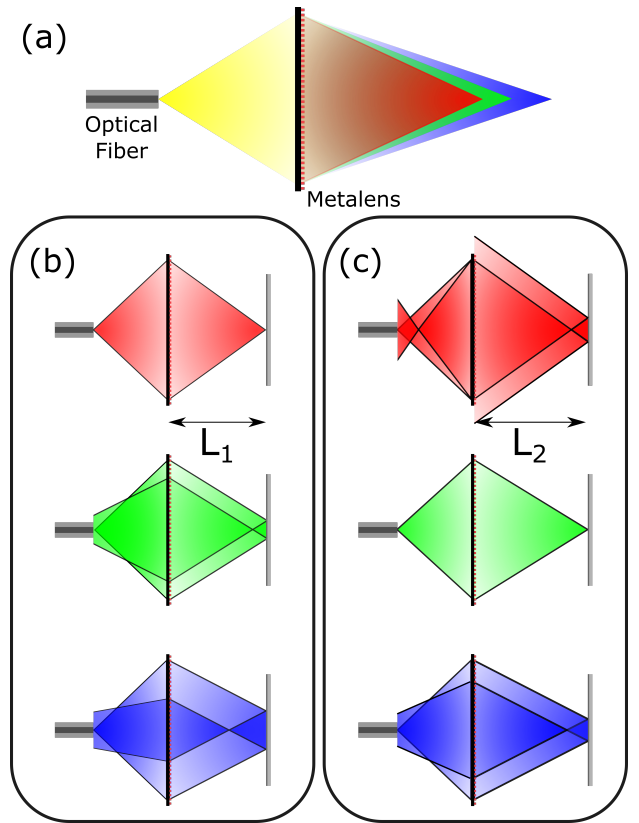

Fig. 1. The operating principle of the chromatic confocal metalens probe. The metasurface takes broadband light from the end of the fiber and focuses different wavelengths to different locations after it. Parts (b) and (c) illustrate the manner in which the broadband light is filtered. In part (b) the red light is in focus on the mirror, and hence refocussed onto the fiber, while the green and blue is out of focus. In part (c) the mirror has moved leading to the green light being focused on the fibre after returning, while the red and blue is out of focus.

work the metalens needed to be combined with a collimating element after the end of the fibre [22]. In this work we present an improved realization, with the metalens designed to function using light directly off the end of an optical fiber allowing the creation of an ultracompact chromatic confocal probe. In this form, the length of the probe is simply that needed to expand the light from the end of the fibre sufficiently and its height and width corresponds to the area of the metasurface used.

Metasurfaces manipulate light using arrays of sub-wavelength nanostructures (meta-atoms) and allow the functionality of a refractive optical element to be achieved without the size and weight of the traditional components. Each individual meta-atom can be selected to facilitate the simultaneous manipulation of the phase, amplitude and polarization of incident light [28], [29]. However, in this work only the manipulation of phase is employed. Furthermore, meta-atoms with rotational symmetry have been chosen by design to minimize their sensitivity to different polarizations. The meta-atoms employed are of the 'truncated waveguide' type [30]–[32], and specifically are cylindrical GaN pillars arranged in a square array of period 450 nm on an Al_2O_3 substrate. By modelling the effect that arrays of pillars with varying

radii have on the light, a set can be identified that allows the phase delay to be varied over 2π. This allows the phase of an arbitrary, but known, incident wavefront to be converted into an arbitrary outgoing wavefront (modulo 2π). The height of all of the pillars on the metasurface is fixed at 750 nm to ease their manufacture, while the 2π variation in the phase delay is achieved by varying the radii from 70 nm to 180 nm in 10 nm steps. The metasurface is designed to focus light with a wavelength of 660 nm to a point 1 mm after the metasurface. If the top of the metasurface lies in the plane $z = 0$, then to produce a spherical wavefront centered on the focal point, the phase of the light after the metasurface should take the following form [31]:

$$\phi(x,y) = -\frac{2\pi}{\lambda}\left(\sqrt{x^2 + y^2 + f^2} - f\right) \quad (\text{mod } 2\pi) \quad (1)$$

where $\phi(x,y)$ is the phase of the light at the point (x,y) on the top of the metasurface, λ is the wavelength of the light and f is the focal length of the metalens. To establish the required phase delay at each point across the metasurface, it is not only the phase after it that needs to be known but also the phase of the incident light. The varying phase delay introduced by the metasurface operates to transform the former into the latter. The phase of the light from the optical fiber is approximated as a point source located at aperture of the fiber. The fiber used is Nufern 460 HP with a quoted mode field diameter of 3.5 ± 0.5 μm at 515 nm, so its approximation to a point source is well justified. The designed spacing between the fibre aperture and the base of the metasurface is 7 mm which, assuming the fibre NA remains close to the quoted value of 0.13, is more than sufficient for the emanating cone of light to expand to cover the entire 1 mm square area of the metasurface. It should be noted that upon reaching the metasurface, the light has been refracted at both the air/Al_2O_3 substrate and the Al_2O_3/GaN interface. The phase of the incident light is calculated by identifying rays that propagate from the point source to the base of each of the pillars of the metasurface and calculating the optical path length along the path. It is assumed that the required phase delay at each point on the metasurface will change the incident phase at the point (x,y) at its base to the target phase at its top at the point (x,y) i.e. the approximation is made that the impact of the metasurface height can be ignored.

All of the steps in the metasurface design consider its effect on light with a wavelength of 660 nm, without considering its impact on other wavelengths. With the pillar structures discussed earlier, eq. 1 is only satisfied at 660 nm. Away from this wavelength, the wavefront is still close to a spherical shape, however the curvature of the wavefront for longer wavelengths is more curved than would be given by eq. 1, leading to light with wavelengths longer than 660 nm being focused closer to the metasurface, while for shorter wavelengths the inverse is true [22]. This is also accompanied by increased lateral chromatic aberration, however a clear focal point is still achieved across the wavelength range considered in this work. Of course, such aberrations are also present when using both DOEs or refractive lenses to achieve the required wavelength-dependent focal position.
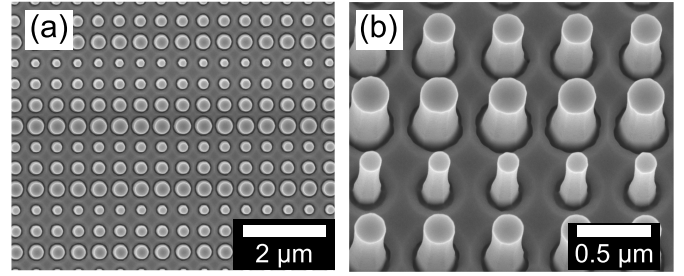

Fig. 2. SEM images of the GaN pillars that make up the metasurface (a) top view; (b) angled view. The pillars are 750 nm high, in a square array of period 450 nm and have radii that vary from 70 nm to 180 nm

The metasurfaces were manufactured using an e-beam and dry etch process by Kelvin Nanotechnology Ltd. (Glasgow) and an SEM image of part of the manufactured metasurface is shown in fig. 2.

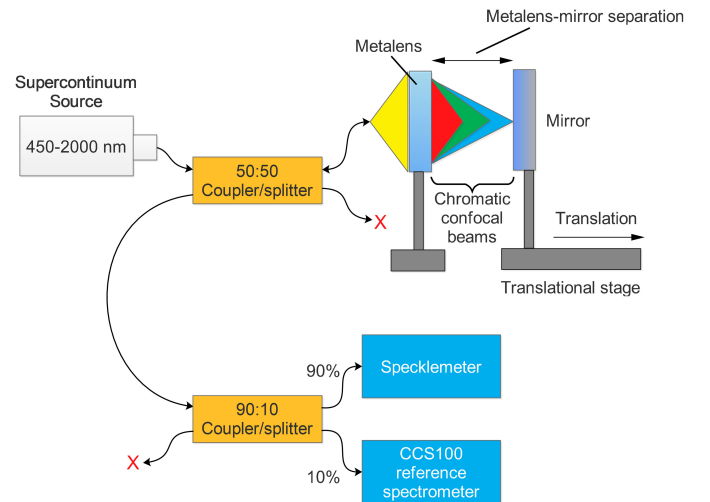### B. Verification of metasurface function using a spectrometer

Fig. 3. A schematic of the experimental setup. Light from a supercontinuum source is coupled into a fibre before passing through a splitter. The light that leaves the end of the fibre, which is considered to approximate a point source, is collected and focused by a metalens with different wavelengths of light being focused to different points along the optical axis. A mirror mounted on a translation stage is scanned along the optical axis leading to different bands of light coupling back into the fibre. The light returning is split, with 90% being directed to the specklemeter, and 10% being directed to a conventional spectrometer to help aid the assessment of the function of the system.

A schematic of the experimental setup is shown in figure 3. A broadband light source (WhiteLase micro, Fianium 450-2000 nm, 60 mW) launched light into a 50:50 coupler/splitter, with half being lost to a beam dump and the other half exiting the fiber and illuminating the metalens. A planar mirror was mounted on a translation stage (MTS25-Z8, Thorlabs) and placed approximately 1 mm after the metalens to act as the object whose location is being measured. The back-scattered light is coupled back into the fiber and passes back through the system, before being divided again. 90% of the returning light power is incident on the specklemeter. The remaining 10% is coupled to a conventional spectrometer (CCS100, Thorlabs)
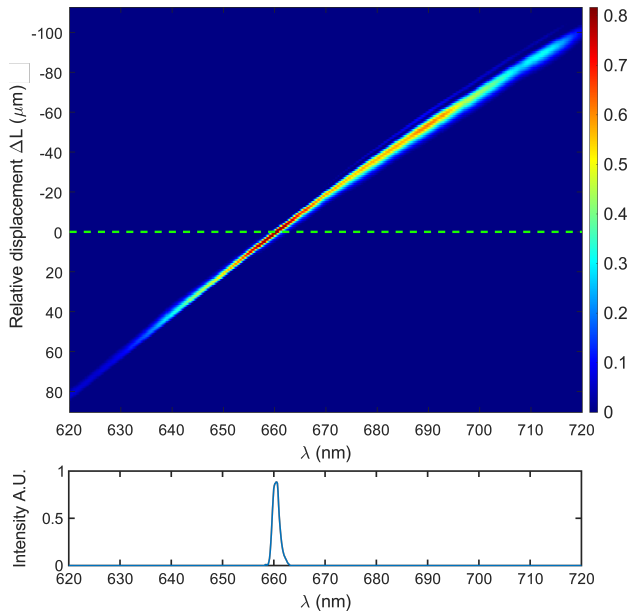
Fig. 4. Part (a) shows how the spectrum of light recorded by the sepctrometer changes as a mirror is scanned along the optical axis. The green line marks the spectra, plotted in part (b), that has its peak closest to the design wavelength of 660 nm.

to determine the precise nature of the signal analysed by the specklemeter.

Figure 4(a) shows a composite plot of the spectra recorded by the CCS100 spectrometer as the mirror is scanned along the z-axis, demonstrating a substantial shift in the peak of the signal returned as the mirror is translated along the optical axis. Part (b) of the figure shows the spectrum recorded for a single mirror position, and corresponds to the results along the green dashed line in part (a). The zero position in the displacement corresponds to a spectral peak at 660 nm, the design wavelength of the lens, and thus the point where the focal point can be expected to be least aberrated. The value of ΔL corresponds to the displacement of the mirror from this point, with positive values corresponding to a shift of the mirror away from the metasurface.

A superposition of the spectra recorded as the mirror is moved along the optical axis in 20 μm steps is shown in fig. 5(a). While the peaks broaden for longer wavelengths the maximum is still easily identified. The variation in the height of the peaks is due to a combination of variations in the source spectrum and the transmission of the metalens at different wavelengths. Part (b) of the figure shows how the peak in the spectrum changes as the mirror is moved along the optical axis. While the change of peak wavelength with mirror position deviates from linear, over this wavelength range it can be seen that the peak wavelength changes on the order of 1 nm every 1.8 μm of displacement.

While the spectrometer provides a clear picture of the light returned across the entire spectrum, it is only location of the spectral peak that is required to identify the position of the measurand. As the spectrometer is often one of the larger and more expensive elements in this arrangement, in the following we look to take an alternative approach, employing a

highly-compact and low-cost speckle pattern-based wavemeter (specklemeter) to detect changes in the signal returned and relate them to position. This allows us to reduce the size and the weight of the overall instrument, leaving both the probe and the detection elements as small devices at either end of an optical fiber, with only the light source needed to be added to provide the fully functional instrument.
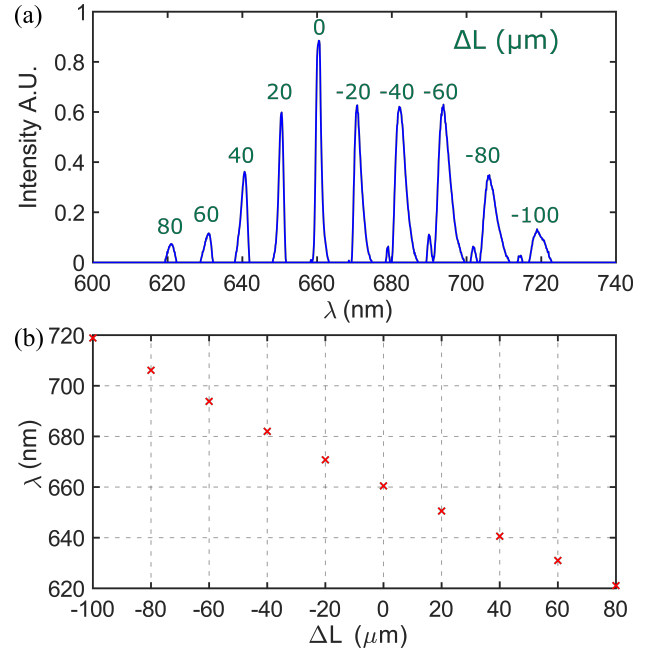

Fig. 5. Part (a) shows a set of the reflection spectra measured by the CCS100 spectrometer at a selection of mirror positions 20μm apart. ΔL corresponds to the distance of the mirror along the optical axis from the point where the peak in the spectra returned occurs at 660 nm. Part (b) shows how the peak wavelength returned changes with the position of the stage.

III. DETERMINING THE REFLECTIVE SURFACE-METALENS DISTANCE BY USING A SCATTERING WAVEMETER

A. The function of the scattering wavemeter

The scattering wavemeter operating principle is based on spectral-to-spatial mapping where the incoming light of a given polarization state and wavelength is converted, through mutual cascade scattering and interference effects, into an observed 2D planar projection (speckle pattern). Despite appearing random, the speckle patterns are in fact highly deterministic and unique for any given input light. In the general case, after calibrating the system over a given wavelength range, an unknown wavelength can be conveniently reconstructed by applying linear algebra techniques [23], [24], [33]. In this work, however, they are directly associated with the position of the measurand without needed into go through this intermediate step. To calibrate the output, the various speckle patterns that are produced as the mirror is scanned along the optical axis are recorded, along with the position of the mirror. Subsequently, the position of a measurand can be directly reconstructed by comparing the generated speckle patterns against these 'reference' speckle patterns. No additional computation is required since all the required information

is already embedded within the speckle patterns. The key challenge in constructing such a system is the development of a suitable scattering medium or 'converter', to generate a unique speckle pattern for each input wavelength.

While scattering wavemeters have major advantages in terms of cost and compactness over conventional optical spectrometers, there can often be significant challenges relating to their stability when subjected to varying environmental conditions. The scattering wavemeter used in this research, however, utilizes a laser-written scattering structure in 'flat fiber' which has high intrinsic stability due to its geometric rigidity and uses both multimode interference and cascade scattering on the scatterer array to mitigate these issues.

B. Flat fiber-based specklemeter assembly

The schematic design of the flat fiber-based specklemeter is shown in fig. 6. The device was made of a section of fussed quartz flat fiber (1 mm × 160 μm × 15 mm) spliced with P1-460B-FC-2 single mode fibre (Thorlabs) which acts as the beam delivery medium. The laser-written scattering structure consisted of 15 planar arrays of pseudo-randomized scattering voids with a vertical separation of 6.6 μm. Each plane comprises 714 × 500 laser-written voids with a randomized position change of ±0.7 μm and an average lateral void separation of 1 μm. The scattering voids were written no closer than 2.5 mm away from the flat fiber-MMF splicing point to ensure the input light will diffract and fill the flat fiber cross-section before reaching the scattering voids. A detailed discussion of scattering voids fabrication was presented in the previous research work by the authors [25]–[27].
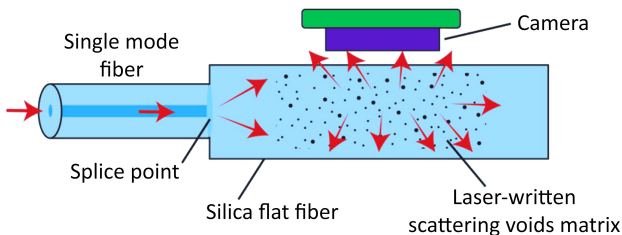

Fig. 6. An illustration of the operation of the flat fiber-based specklemeter where the input light, delivered by single mode fiber, diffracts and reaches the scattering voids matrix. The scattered light is captured on the top-mounted camera detector

A modified Raspberry Pi V2 NoIR camera module, having its lens removed to yield a bare Sony IMX219 CMOS sensor, acts as the speckle pattern detector. It was mounted on the top of the scattering structure to allow ballistic light to bypass the detector, thus providing background free speckles. The system was enclosed in the monocoque 3D printed box (Tough PLA, Ultimaker) with dimensions of 2.5 × 2.5 × 2.5 cm. It is worth noting the box size was limited by the fixed-size of the camera board itself, so further integration of the systems in an even smaller footprint is possible by using smaller footprint camera module.

C. Calibration of the Specklemeter

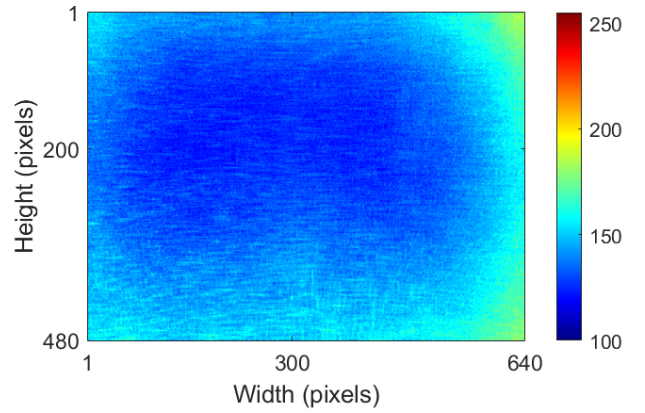Speckle patterns were recorded as the mirror was scanned over a 227 μm range, shifting from 114 μm before the point

Fig. 7. Exemplar pseudo-colored 640 × 480 pixels speckle pattern generated from the flat fiber-based device with a 1 mm metalens-mirror separation. The colorbar indicates the 8-bit pixel values

where the peak in the spectra returned was at 660 nm, as measured by the spectrometer, to 113 μm after it in 1 μm steps. For each stage position the speckle pattern images were captured with fixed camera exposure (ISO=200, shutter speed=0.5 s). Each speckle pattern was captured as an 8-bit RGB 640 × 480 pixels PNG file. An exemplar speckle pattern is presented in fig. 7. Two experimental runs were completed, the first for calibration and the second a measurement set that is subsequently analysed using the calibrated specklemeter, with 650 speckle patterns being captured for each dataset. Each speckle pattern image is initially processed by: a) converting the image to grayscale; b) normalising the pixel values to floating point values in a range between 0-1; c) performing vectorization by stacking each consecutive image column to the bottom of the previous one. The resulting image is represented as vector with 307200 × 1 elements. Once all images were processed in this way, a matrix is formed by concatenating the image vector as consecutive columns. In total two matrices were generated one for each of the calibration and measurement datasets respectively.

The next step was to perform a machine learning-based principal component analysis (PCA) on the calibration dataset [34]–[36]. The calibration data matrix was further processed to meet the requirements of the PCA analysis as follows: the matrix was transposed such that the number of rows corresponding to the number of observations, and the number of columns matches the total pixel number per speckle (307200); b) the average row was computed and subtracted from the matrix to create a mean-centered matrix X; c) singular value decomposition (SVD) was applied to the modified calibration data to derive three matrices: U, Σ, V (eq. 2).

$$X \xrightarrow{SVD} U, \Sigma, V \quad \text{and} \quad X = U\Sigma V^T \qquad (2)$$

The dot-product between the U (eigenfunctions) and Σ (singular value 'weights') results in a matrix P_{PCA} with the same dimensions as the input matrix but with its columns describing the changes in the system in hierarchical order from the most to the least significant by variation. The contribution of each column is described in the matrix V, and these contributing

factors are called loadings (eq. 3). The values represented by each column in the matrix, P_{PCA} are called principal components. There are as many sets of these as the total number of variables i.e. number of pixels in the speckle pattern image.

$$P_{\mathrm{PCA}} = U\Sigma \quad \text{and} \quad \text{Loadings} = V \tag{3}$$

By selecting a given component set (column), the data can be projected onto a lower-dimensional space, revealing the 'masked' trend obfuscated by either the correlation (similarity) limit or environmental instabilities. Thus, by selecting the given column from P_{PCA}, the high-dimensionality of the total pixel number will be reduced to a single dimension, and the resulting 'projection' vector has a length of total sample number. After the calibration dataset has been processed in this manner, the selected components can be subsequently applied to realise measurement data matrix projections which forms the basis for obtaining a measurement result. The final step of the PCA-based analysis is to cross-compare the projected datasets and to translate the projection values to the measurands with the help of reference obtained during calibration.

The reconstruction of the mirror's location from the speckle patterns as it is shifted along the optical axis in 1 μm steps is shown in the fig. 8. The PCA1 projection (first column of the principal components matrix P_{PCA}) was selected for both the calibration and measurements datasets because it follows the linear trend of increasing separation distance between the metalens and the mirror. While in a perfect scenario, both trends should perfectly overlap, there is a mismatch between the calibration and measurement PCA1 projections with a standard deviation of 0.65 μm and a worst-case deviation of 1.61 μm. Similarly, the reconstruction from the PCA1 values to the reference separation distance confirms the same trend with the standard deviation reconstruction error of 1.37 μm with a maximum deviation of 3.60 μm as shown in fig. 8(b). The distance reconstruction error, shown in fig. 8(c) implies the presence of a systematic error as, instead of being random, it appears to jump between two solutions, leading to oscillations of approximately 2.1 μm. This error most likely arises due to the coarse sampling of the calibration speckle patterns, with the set consisting of measurements taken at 1 μm steps. It is likely that the measurement results would improve if a finer sampling was taken for the calibration data, or if a deeper analysis of the PCA results were carried out.

IV. DISCUSSION

A. Impact of the shape of the spectra

While with the spectrometer the result at each wavelength is separated out, allowing the peak reflected wavelength to be easily identified, with the specklemeter the results of all the returned wavelengths are superimposed in the image that is generated, and the impact of the broadened spectra on the speckle pattern formation and subsequent analysis needs to be considered. The broadened spectral peak will result in the speckle patterns from all of the contributing wavelengths being superimposed in the image recorded by the camera, leading to a less well-defined speckle pattern than is formed
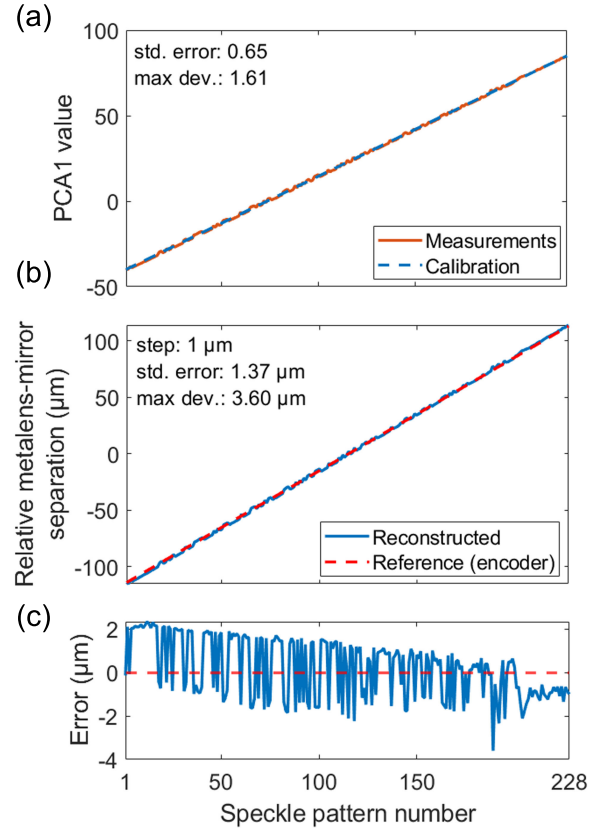

Fig. 8. Metalens-reflective mirror separation distance reconstruction results: (a) the first principal component projection (PCA1) for calibration (dashed) and measurement (solid) datasets as separation distance increases. (b) the reconstructed distance (solid) and reference measurement as given by the encoder (dashed). (c) a plot of the error across the measurement range. The standard reconstruction error equals 1.37 μm with a maximum deviation of 3.60 μm.

for monochromatic light as the highly wavelength dependant speckle patterns begin to average out. In addition, the SNR of the given spectrum also plays an important role. For a higher SNR, more information related to the peak wavelength is contained in the speckle pattern. However, we have shown that the bandwidth of the returned light is sufficiently narrow that the measurand position can still be determined from the non-ideal (i.e. non-monochromatic) spectral peaks that result from the superimposed speckles. Indeed is has been shown that the specklemeter based system can be used to identify the location of the mirror over the entire operational range that was demonstrated above when using the spectrometer. The results were reconstructed via PCA projection with 1.37 μm standard error and a worst-case deviation of 3.6 μm despite the varying spectra shapes and signal-to-noise ratios that can be seen in the signals recorded by the reference spectrometer (illustrated in fig. 5(a)). If the axial shift of the focal point with wavelength was increased through modifications to the design of the metasurface, then a narrower band of light would be collected which should lead to an improved performance of the specklemeter.

B. Scope for Specklemeter improvement

The speckle pattern-based wavemeter, acting as the interrogator, had a total size of 2.5 × 2.5 × 2.5 cm and a weight of 160 g. Its detector was made of a modified Raspberry Pi V2 NoIR camera with a lens removed and fixed exposure of 0.5s shutter speed and ISO=200. Here, the system limit is the sampling rate which is determined by the 0.5s shutter speed to 2 Hz. The rationale for these exposure parameters was to compensate for low optical power reaching the detector (6.3 μW). This can be further modified by replacing the 50:50 splitter in the setup with a circulator, which will increase the optical power delivered to the detector, thus reducing the required shutter speed.

C. Scope for improvement in the metasurface probe

The metalens used in the probe was designed to focus light with a wavelength of 660 nm to a point 1 mm after the metasurface, with its performance at other wavelengths just being that which the chosen form of dielectric pillars used deliver. While the function at these other wavelengths was tested through simulation before its construction, if alternate pillar parameters had been chosen the performance at wavelengths away from 660 nm may be different, even while its performance at this wavelength is maintained. Thus if the meta-atoms are modified it is possibly to change the range and resolution that such a probe will deliver. Altering the structures of the metasurface will also change such things as the level of transmission of the light at the different wavelengths altering the range of wavelengths that such a probe will work well for. For the system here is was demonstrated that, even when only 10% of the light returned after passing through the 50:50 splitter is sent to the spectrometer, the operating wavelength range covers 620 nm-720 nm without significant issue.

D. Metasurfaces as a platform for wider instrument miniaturisation

While in this work we have shown that metasurfaces offer a route by which more compact chromatic confocal probes can be realised, the advantages that these metasurfaces offer are not just restricted to this technique. The wavefront manipulations achievable go beyond just the focusing of light, as each metasurface allows the simultaneous modification of the phase, polarisation and amplitude of light as it passes through it. This offers a path by which the number of elements needed in optical instrumentation can be reduced, and those elements which are used can be realised in an ultra-compact and lightweight form. This may be particularly effective in monochromatic techniques, though more complex metasurface designs [28], [37], [38], or designs exploiting multiple metasurfaces [39]–[41], can be used to achieve the desired phase delay over a broader band of light. By using metasurfaces as a platform to achieve a step-change in instrument size and weight a more general shift to instrumentation suitable for on-machine and in-process measurements can be realised.

V. CONCLUSION

We have demonstrated that the spectrometer in a chromatic confocal sensor can be replaced with a low cost and compact specklemeter with good performance still being achieved. By implementing this with a chromatic confocal probe that is formed from just a metasurface being combined with the end of an optical fiber to act as a pinhole, the entire instrument can be realised in an ultra-compact form and one which is in an ideal form for use for on-machine and in-process measurements where other optical instrumentation may not fit. In the implementation here we have included an additional splitter to send 10% of the light into a traditional spectrometer allowing the full spectrum to be viewed as the performance of the specklemeter is examined, and allowing the performance of the metasurface based probe in filtering the input spectrum to be assessed. Even though the light returned into the detector has a range of wavelengths present, the specklemeter is able to distinguish the differences between the light returned in each case sufficently well for this application. The reconstruction of the distance information from collected speckle patterns was possible by applying PCA projection, which resulted in the successful recovery of the location of the mirror over a 227 μm range with a standard deviation in the position error of 1.37 μm, and a maximum deviation of 3.6μm, and could likely be improved on with additional development of the metasurface probe, and with an improved calibration of the specklemeter with more finely sampled data and a more in depth analysis of the PCA results.

For the purpose of open access, the author(s) has applied a Creative Commons Attribution (CC BY) license to any Accepted Manuscript version arising

REFERENCES

[1] D. Li, B. Wang, Z. Tong, L. Blunt, and X. Jiang, "On-machine surface measurement and applications for ultra-precision machining: a state-of-the-art review," *The International Journal of Advanced Manufacturing Technology*, vol. 104, pp. 831–847, 2019.

[2] X. Wu, L. Zhu, F. Fang, and X. Zhang, "Research on the quality control technology of micro-topography machining based on in situ white light interferometry," *Measurement*, vol. 220, p. 113257, 2023.

[3] M. Xi, Y. Wang, H. Liu, H. Xiao, X. Li, H. Li, Z. Ding, and Z. Jia, "Calibration of beam vector deviation for four-axis precision on-machine measurement using chromatic confocal probe," *Measurement*, vol. 194, p. 111011, 2022.

[4] R. Meeß, D. Dontsov, and E. Langlotz, "Interferometric device for the in-process measurement of diameter variation in the manufacture of ultraprecise spheres," *Measurement Science and Technology*, vol. 32, no. 7, p. 074004, 2021.

[5] W. Gao, H. Haitjema, F. Fang, R. Leach, C. Cheung, E. Savio, and J.-M. Linares, "On-machine and in-process surface metrology for precision manufacturing," *CIRP Annals*, vol. 68, no. 2, pp. 843–866, 2019.

[6] M. Javaid, A. Haleem, R. P. Singh, S. Rab, and R. Suman, "Significance of sensors for industry 4.0: Roles, capabilities, and applications," *Sensors International*, vol. 2, p. 100110, 2021.

[7] V. Azamfirei, F. Psarommatis, and Y. Lagrosen, "Application of automation for in-line quality inspection, a zero-defect manufacturing approach," *Journal of Manufacturing Systems*, vol. 67, pp. 1–22, 2023.

[8] A. Henning, D. Townend, H. Martin, and X. J. Jiang, "Metasurface-based ultracompact instrumentation to support future smart manufacturing," in *Optics and Photonics for Advanced Dimensional Metrology II*. SPIE, 2022, p. PC1213706.

[9] X. Jiang and A. Henning, "Precision metrology: from bulk optics towards metasurface optics," *Contemporary Physics*, vol. 62, no. 4, pp. 199–216, 2021.

[10] F. Blateyron, "Chromatic confocal microscopy," in *Optical Measurement of Surface Topography*, R. Leach, Ed. Berlin, Heidelberg: Springer Berlin Heidelberg, 2011, pp. 71–106. [Online]. Available: https://doi.org/10.1007/978-3-642-12012-1_5

[11] Y. Ma, Y. Xiao, Q. Wang, K. Yao, X. Wang, Y. Zhou, Y. Liu, Y. Sun, and J. Duan, "Applications of chromatic confocal technology in precision geometric measurement of workpieces," in *Journal of Physics: Conference Series*, vol. 2460, no. 1. IOP Publishing, 2023, p. 012077.

[12] Y. Wang, M. Xi, H. Liu, Z. Ding, W. Du, X. Meng, Y. Sui, J. Li, and Z. Jia, "On-machine noncontact scanning of high-gradient freeform surface using chromatic confocal probe on diamond turning machine," *Optics & Laser Technology*, vol. 134, p. 106569, 2021.

[13] X. Zou, X. Zhao, G. Li, Z. Li, and T. Sun, "Non-contact on-machine measurement using a chromatic confocal probe for an ultra-precision turning machine," *The International Journal of Advanced Manufacturing Technology*, vol. 90, pp. 2163–2172, 2017.

[14] Q. Yu, Y. Zhang, W. Shang, S. Dong, C. Wang, Y. Wang, T. Liu, and F. Cheng, "Thickness measurement for glass slides based on chromatic confocal microscopy with inclined illumination," in *Photonics*, vol. 8, no. 5. MDPI, 2021, p. 170.

[15] L. Ye, J. Qian, H. Haitjema, and D. Reynaerts, "On-machine chromatic confocal measurement for micro-edm drilling and milling," *Precision Engineering*, vol. 76, pp. 110–123, 2022.

[16] S. Fu, W. S. Kor, F. Cheng, and L. K. Seah, "In-situ measurement of surface roughness using chromatic confocal sensor," *Procedia CIRP*, vol. 94, pp. 780–784, 2020.

[17] M. Hillenbrand, B. Mitschunas, F. Brill, A. Grewe, and S. Sinzinger, "Spectral characteristics of chromatic confocal imaging systems," *Applied Optics*, vol. 53, no. 32, pp. 7634–7642, 2014.

[18] T. Wilson, "Scanning optical microscopy," *Scanning*, vol. 7, no. 2, pp. 79–87, 1985.

[19] G. S. Kino and T. R. Corle, *Confocal scanning optical microscopy and related imaging systems*. Academic Press, 1996.

[20] C. Sheppard, *Confocal microscopy: Principles, practice and options*. Academic Press, London, UK, 1999.

[21] M. Gu, *Principles of three dimensional imaging in confocal microscopes*. World Scientific, 1996.

[22] J. Chan, D. Tang, J. Williamson, H. Martin, A. Henning, and X. Jiang, "An ultra-compact metasurface-based chromatic confocal sensor," *CIRP Annals*, 2023.

[23] B. Redding, S. M. Popoff, and H. Cao, "All-fiber spectrometer based on speckle pattern reconstruction," *Optics express*, vol. 21, no. 5, pp. 6584–6600, 2013.

[24] B. Redding, S. F. Liew, R. Sarma, and H. Cao, "Compact spectrometer based on a disordered photonic chip," *Nature Photonics*, vol. 7, no. 9, pp. 746–751, 2013.

[25] P. Falak, T. Lee, S. Zahertar, B. Shi, B. Moog, G. Brambilla, C. Holmes, and M. Beresna, "Compact high-resolution FBG strain interrogator based on laser-written 3D scattering structure in flat optical fiber," *Scientific Reports*, vol. 13, no. 1, p. 8805, May 2023. [Online]. Available: https://doi.org/10.1038/s41598-023-35708-1

[26] Q. Sun, P. Falak, T. Vettenburg, T. Lee, D. B. Phillips, G. Brambilla, and M. Beresna, "Compact nano-void spectrometer based on a stable engineered scattering system," *Photon. Res.*, vol. 10, no. 10, pp. 2328–2336, Oct 2022. [Online]. Available: https://opg.optica.org/prj/abstract.cfm?URI=prj-10-10-2328

[27] Q. Sun, J. Williamson, T. Vettenburg, D. B. Phillips, H. Martin, G. Brambilla, X. Jiang, and M. Beresna, "A scattering spectrometer for white light interferometry," *Optics and Lasers in Engineering*, vol. 169, p. 107743, 2023. [Online]. Available: https://www.sciencedirect.com/science/article/pii/S0143816623002725

[28] W. T. Chen, A. Y. Zhu, V. Sanjeev, M. Khorasaninejad, Z. Shi, E. Lee, and F. Capasso, "A broadband achromatic metalens for focusing and imaging in the visible," *Nature nanotechnology*, vol. 13, no. 3, pp. 220–226, 2018.

[29] N. Yu and F. Capasso, "Flat optics with designer metasurfaces," *Nature materials*, vol. 13, no. 2, pp. 139–150, 2014.

[30] P. Lalanne, S. Astilean, P. Chavel, E. Cambril, and H. Launois, "Design and fabrication of blazed binary diffractive elements with sampling periods smaller than the structural cutoff," *JOSA A*, vol. 16, no. 5, pp. 1143–1156, 1999.

[31] M. Khorasaninejad and F. Capasso, "Metalenses: Versatile multifunctional photonic components," *Science*, vol. 358, no. 6367, p. eaam8100, 2017.

[32] X. Luo, "Engineering optics 2.0: a revolution in optical materials, devices, and systems," *Acs Photonics*, vol. 5, no. 12, pp. 4724–4738, 2018.

[33] B. Redding, S. M. Popoff, Y. Bromberg, M. A. Choma, and H. Cao, "Noise analysis of spectrometers based on speckle pattern reconstruction," *Applied optics*, vol. 53, no. 3, pp. 410–417, 2014.

[34] S. L. Brunton and J. N. Kutz, "Singular Value Decomposition (SVD)," in *Data-Driven Science and Engineering: Machine Learning, Dynamical Systems, and Control*. Cambridge University Press, 2019, p. 3–46.

[35] G. D. Bruce, L. O'Donnell, M. Chen, and K. Dholakia, "Overcoming the speckle correlation limit to achieve a fiber wavemeter with attometer resolution," *Opt. Lett.*, vol. 44, no. 6, pp. 1367–1370, Mar 2019. [Online]. Available: https://opg.optica.org/ol/abstract.cfm?URI=ol-44-6-1367

[36] S. Ng, "Principal component analysis to reduce dimension on digital image," *Procedia Computer Science*, vol. 111, pp. 113–119, 2017, the 8th International Conference on Advances in Information Technology. [Online]. Available: https://www.sciencedirect.com/science/article/pii/S1877050917311900

[37] S. Wang, P. C. Wu, V.-C. Su, Y.-C. Lai, M.-K. Chen, H. Y. Kuo, B. H. Chen, Y. H. Chen, T.-T. Huang, J.-H. Wang *et al.*, "A broadband achromatic metalens in the visible," *Nature nanotechnology*, vol. 13, no. 3, pp. 227–232, 2018.

[38] W. T. Chen, A. Y. Zhu, J. Sisler, Z. Bharwani, and F. Capasso, "A broadband achromatic polarization-insensitive metalens consisting of anisotropic nanostructures," *Nature communications*, vol. 10, no. 1, p. 355, 2019.

[39] B. Groever, W. T. Chen, and F. Capasso, "Meta-lens doublet in the visible region," *Nano letters*, vol. 17, no. 8, pp. 4902–4907, 2017.

[40] C. Kim, S.-J. Kim, and B. Lee, "Doublet metalens design for high numerical aperture and simultaneous correction of chromatic and monochromatic aberrations," *Optics Express*, vol. 28, no. 12, pp. 18 059–18 076, 2020.

[41] Y. Zhou, I. I. Kravchenko, H. Wang, J. R. Nolen, G. Gu, and J. Valentine, "Multilayer noninteracting dielectric metasurfaces for multiwavelength metaoptics," *Nano letters*, vol. 18, no. 12, pp. 7529–7537, 2018.

Data Availability